Archive of Applied Mechanics (2023) 93:2533–2547
https://doi.org/10.1007/s00419-023-02395-3

ORIGINAL

Galal M. Moatimid · T. S. Amer · Marwa H. Zekry

Analytical and numerical study of a vibrating magnetic inverted pendulum

Received: 28 September 2022 / Accepted: 25 February 2023 / Published online: 19 March 2023

Abstract The current study investigates the stability structure of the base periodic motion of an inverted pendulum (IP). A uniform magnetic field affects the motion in the direction of the plane configuration. Furthermore, a non-conservative force as one that dampens air is considered. Its underlying equation of motion is derived from traditional analytical mechanics. The mathematical analysis is made simpler by substituting the Taylor theory in order to expand the restoring forces. The modified Homotopy perturbation method (HPM) is employed to achieve a roughly adequate regular result. To support the prior result, a numerical method based on the fourth-order Runge-Kutta method (RK4) is employed. The graphs for both the analytic and numerical solutions are highly consistent with one another, which indicates that the perturbation strategy is accurate. The solution time history curve exhibits a decaying performance and indicates that it is steady and without chaos. The resonance and non-resonance cases are found through the stability study by using the time scale method. In all perturbation approaches, the methodology of multiple time scales is actually regarded as a further standard approach. The time history is used to create a collection of graphs. Some graphical representations are used to illustrate how the typical physical values affect the behavior of the discovered solution. It has been discovered that the statically unstable IP can have its instability reduced by raising the spring torsional constant stiffness as well as the damped coefficient. Moreover, the magnetic field has a significant role in the stability configuration, which explains that at higher values of this field, the decaying waves take much more time than the smaller values of this field. Accordingly, it can be employed in various engineering devices that need a certain period of time to be more stable.

Keywords Inverted pendulum · Magnetic field · Parametric excitation · Homotopy perturbation method · Multiple time scales method

1 Introduction

In the control theory and experimentation, the IP signifies a vital aspect. Numerous physical models, such as rockets, can be characterized as flexible IPs. Many present studies focus exclusively on rigid instances, despite the fact that rigid models are simply an approximation of elastic bodies. Rigid models are incompetent in

G. M. Moatimid
Department of Mathematics, Faculty of Education, Ain Shams University, Cairo, Egypt
e-mail: gal_moa@edu.asu.edu.eg

T. S. Amer (✉)
Department of Mathematics, Faculty of Science, Tanta University, Tanta 31527, Egypt
e-mail: tarek.saleh@science.tanta.edu.eg

M. H. Zekry
Department of Mathematics and Computer Science, Faculty of Science, Beni-Suef University, Beni-Suef, Egypt
e-mail: marwa.zekry@science.bsu.edu.eg

accurately describing the kinetic features of real-world systems. When high-frequency disturbances disrupt the system, the controllers established on the small-frequency estimate prototype are unable to stabilize it. Due to the approximation, the features of elastic systems differ significantly from those of rigid systems. Because traditional approaches presume that the flexible structure is a rigid prototype, they are inadequate in more complicated engineering situations. A new kind of IP, elastic IP, was planned, and flexibility was investigated [1]. The Mathematical prototype originated from the Hamiltonian theory and variational techniques, which were created by a combination of partial and ordinary differential equations. The prototypical nonlinear and the completely unstable system is an IP. An optimization model of an IP procedure depending on the vision motion was suggested to control the triple IP successfully and steadily [2]. The IPs can be thought of as a close approximation to the problem of robot stability. A hypothetical and investigational foundation for estimating the system speed and distortion was investigated [3]. The Hamiltonian canonical equation was used to investigate the chaotic dynamics of a double IP with a large swing angle [4]. The research led to new concepts and theoretical foundations for chaotic dynamics analysis in the sectors of aircraft, electronics, and biological manufacturing. A semi-analytical approach to explore the stability and bifurcation of the IP with periodic motions was used [5]. It was demonstrated that the stability of IP could be predicated on the periodic motion of its base. Nonlinear fluctuations of a rotatory IP with a full-state feedback control were examined [6]. The theoretical conclusions of the nonlinear vibrations of the rotary IP are confirmed by experimental quantities, and the findings of both methodologies show remarkable agreement. Using a combination of Lab VIEW and MATLAB algorithms, the animation software simulations built a realistic triple IP model [7]. The swinging of the pendulum and the entire traveling procedure of the cart were seen in multi-dimensional and multi-angle simulations. The strategy introduced a new research platform for IP simulation that is observable. The work of Johnson et al. [8] enhanced perceptive controls for uses other than IP, like human motion. If these technologies are successful, it would be much easier to argue that perception control theory adequately explains how living creatures behave.

The concept of parametric excitation seemed to be another important issue in dynamics. When at least one of the parameters in the equation of motion is clearly dependent on time, this concept arises. The stiffness of the harmonic oscillation, around a non-zero value in a linear system, was a historically specific oscillator regulated by Mathieu's equation. In this case, the Floquet theory can be used to show the stability of a given pair of stiffness fluctuation frequency and amplitude. The existence of unconstrained solutions to Mathieu's equation is more likely in the situation of primary parametric instability, which happens when the parametric excitation frequency is double that of the normal frequency. A more detailed analysis of Mathieu's equation was earlier shown [9, 10]. The dynamical behavior of a floating body in the presence of parametric resonances was studied [11]. It was discovered that the presence of stable quasiperiodic motions agreed with both pitch and heave resonance. A model was established on the specific nonlinear Froude–Krylov strength computation that was used to qualitatively validate the results. The vibrating motion of an automatic parametric pendulum coupled to a damped system was studied [12–15]. The kinematic equations of the system were obtained using Lagrange's equations in agreement with their generalized coordinates. A wide-ranging examination of variable-length pendulums was presented [16]. Using mathematical modeling, dynamical analysis, and innovative computer simulations, an attempt at a unique evaluation of current advancements in this domain was made. Major developments were addressed of many notions and their theoretical and engineering applications. Dedicated numerical approaches were used to verify some key physical ideas, which were evaluated utilizing dynamical analysis. Multi-harmonic resonances were widespread in rotor systems and had a major impact on their nonlinear properties [17]. The convergence of the conclusions and the confirmation of the solutions with the existing literature data were provided. The nonlinear mathematical model was used to discover nonlinear and double-factor chaotic fluctuations for the construction under a combination of aerodynamic intensity and variable spinning velocity [18]. The parameterized and external resonances were used to simplify the variable rotational speed and aerodynamic force, respectively. Membranes have been commonly employed in long-span pitches and other constructions due to their light and flexibility qualities [19]. External loads, on the other hand, will result in a rather substantial displacement. Consequently, experts have been concerned about the substantial deviation oscillation of the membranes. It should be noted that the existing problem of an IP reveals the presence of periodic circular functions which arise due to its periodic move bases.

Perturbation methods, which are extensively used techniques, were of remarkable interest for use in engineering and many areas of practical physics. A novel strategy founded on homotopy terminology has been developed to overcome the limitation of a small parameter (SP) which inevitably exists in all perturbation methodologies. Consequently, the methodology of the new approach was given the name (HPM). The Chinese Mathematician Prof. He [20] was the first who proposed the HPM. Therefore, without utilizing the perturba-

tion procedure, a nonlinear challenge was reduced to an endless set of easy complications. Allowing the SP to proceed from zero to unity effectively converts the problem into a particular perturbation problem with a little embedded factor. Many studies showed the powerful effectiveness of the new technique [21–23]. The classic perturbation methodology and homotopy analysis method can be fully utilized in this approach. The new approach has been used for ordinary as well as partial differential equations in both linear and nonlinear features. It has been used to solve a wide range of different forms of differential equations. When compared to other perturbation methods, the HPM clearly generates better accurate outcomes. Consequently, the HPM offers all the advances of traditional perturbation methods without the necessity of SP in the solution technique. The method has an easier form than the prior classical approaches because it requires less computation time and has higher computational precision. The method takes only initial conditions to solve any problem and gives an analytical approximate solution to the structure of an infinite power series. A lot of researchers employed HPM to solve nonlinear differential equations, and their results have been conveniently reported. Considering the HPM, the accurate solution of the Duffing equation was achieved [24]. This equation has considerable significance in biology, manufacturing, physics, and communication hypothesis. The motion of a sliding particle on a smooth upright parabola was investigated [25]. An analytic bounded solution was obtained by combining the HPM and the Laplace transforms. In accordance with the effectiveness and accuracy of the HPM, a modified approach is utilized throughout the current paper.

In light of the aforementioned aspects, this paper focuses on the vibrating dynamical motion of IP. The current work attempts to provide an overview of the nonlinear mechanism concept, established on its straightforward form and rich nonlinear prototype. Typically, the IP is statically unstable in its initial state in view of the gravitational attraction. Therefore, it is subjected to a light torsional spring, which is associated with the IP with the vertically upward axis. According to the potential purposes of the presence of the magnetic strength, the IP is affected by an unchanged magnetic field, which is orthogonal to the vertical plane containing the IP.

The following questions should have their answers at the conclusion of this investigation:

- How can an accurate approximate solution consistent with RK4 be found?
- What is about the stability analysis in resonance and non-resonance situations?
- What are the influences of the different physical factors on the stability profile?
- How can the static instability of the IP be suppressed?

The remainder of the current work is constructed as follows: The regulating equation of motion of the magnetic IP is derived in Sect. 2. Section 3 is devoted to introducing the application of the frequency equivalence technique as a novel procedure to the stability analysis as well as the approximate solution of the given IP. The relationship connecting the numerical and analytical solutions displays the good precision of the used perturbation method. The non-resonance as well as the resonance cases are examined. Some plots are given to show the impact of different factors on the examined motion. Finally, the concluded remarks are drawn in Sect. 4.

2 Physical modeling of the IP

As shown in Fig. 1, a sketch of an excited parametric IP is displayed. For more convenience, the Cartesian coordinates $(x,\ y,\ z)$ will be utilized to modulate the physical prototype. The system contains a bob which, for simplicity, is treated as a point with the mass m and connected to a mass-less rigid rod of length L to the pivot, which is located at the origin of the frame of reference O. This pivot has a periodic movement as the periodic function $Q_0 \cos \Omega t$, where Q_0 and Ω are the movement amplitude and frequency, respectively. As seen, the considered IP rotates along with the vertical $xy-$ plane, where $\underline{i}$ and $\underline{j}$ are unit vectors along the $x-$ and $y-$ axis, correspondingly. Simultaneously, the unit vector $\underline{k}$ acts along with the normal $z-$ direction. At this stage, the IP is fundamentally unstable, where it is hung above the horizontal plane, and it will go down by the gravitational impacts. Therefore, a light torsional spring of stiffness k is attached to the vertical axis from the IP. Additionally, an air-damping force with a damped coefficient δ to the horizontal direction is considered. Moreover, a uniform magnetic field $B\,\underline{k}$ acting along with the negative $z-$ direction is considered. The fundamental goal of the considered control system is to address the stability of the IP.

In light of the previous simplified description, the governing equation of motion may be considered as a particle of mass m, which moves in the $xy-$ plane and subjected to a normal uniform magnetic field. Therefore, the position vector of the mass m may be written as:

$$\underline{r} = (L\ \sin\theta + Q_0 \cos \Omega t)\,\underline{i} + L \cos\theta\ \underline{j}\,, \tag{1}$$

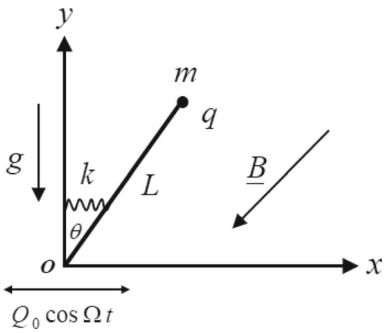

Fig. 1 Sketches the IP with a horizontal periodic moving base

where $\underline{i}$ and $\underline{j}$ are the unit vectors in the paths of x and y axes. It follows that its velocity may be given by

$$\underline{v} = (L\dot{\theta}\,\cos\theta - \Omega Q_0 \sin \Omega t)\,\underline{i} - L\dot{\theta}\sin\theta\,\underline{j}, \tag{2}$$

where the dot sign stands for the differentiation with time.

The kinetic energy of the point mass is addressed as follows:

$$T = \frac{m}{2}[L^2\dot{\theta}^2 - 2L\Omega Q_0\dot{\theta}\cos\theta\sin\Omega t + \Omega^2 Q_0^2 \sin^2 \Omega t]. \tag{3}$$

Actually, the potential energy results from different activities; these circumstances may be classified as follows:

- The gravitational potential energy, which gives the energy of an object concerning a gravitational field, is characterized as $mgL\cos\theta$.
- The elastic potential energy is the potential energy which results from the distortion of an adaptable body, such as the spring enlargement. It is a prime example of the work done by stretching the spring. It depends upon the stiffness of the spring constant k and the reduced distance. It may be formulated as: $k\theta^2/2$.
- The charged IP moves in a uniform magnetic field $\underline{B} = B\,\underline{k}$; therefore, the potential function of the problem must include the magnetic term $q\,\underline{P}\,.\,\underline{v}$, where $\underline{P}$ is the magnetic vector potential; for instance, see Eyal and Goldstein [26]. Keep in mind that the relationship between the magnetic field $\underline{B}$ and the magnetic potential $\underline{P}$ is given by: $\underline{B} = \nabla \wedge \underline{P}$. One may show that one of the possibilities of the vector potential is given by $\underline{P} = \frac{1}{2}\left(\underline{B} \wedge \underline{r}\right)$. It follows that $\underline{P}$ can be expressed as:

$$\underline{P} = \tfrac{1}{2}B[-L\cos\theta\,\underline{i} + (L\sin\theta + Q_0\cos\Omega t)\,\underline{j}]. \tag{4}$$

Combining Eqs. (2) and (4), the potential energy due to the uniform magnetic field may be formulated as follows:

$$P.E_{mag} = -\tfrac{1}{2}qlB[L\dot{\theta} + Q_0\dot{\theta}\sin\theta\cos\Omega t - \Omega Q_0\cos\theta\sin\Omega t]. \tag{5}$$

Consequently, the total potential energy may be expressed as follows:

$$V = mgL\cos\theta + \tfrac{1}{2}k\theta^2 - \tfrac{1}{2}qLB\left[L\dot{\theta} + Q_0\dot{\theta}\sin\theta\cos\Omega t - \Omega Q_0\cos\theta\sin\Omega t\right]. \tag{6}$$

Combining Eqs. (3) and (5), it follows that the Lagrangian function of the considered magnetic IP is given by

$$\begin{aligned}\Re &= T - V\\ &= \frac{1}{2}m[L^2\dot{\theta}^2 - 2L\Omega Q_0\dot{\theta}\cos\theta\sin\Omega t + \Omega^2 Q_0^2\sin^2\Omega t] - [mgL\cos\theta\\ &\quad + \frac{1}{2}k\theta^2 - \frac{1}{2}qLB(L\dot{\theta} + Q_0\dot{\theta}\sin\theta\cos\Omega t - \Omega Q_0\cos\theta\sin\Omega t)].\end{aligned} \tag{7}$$

The air-damping force can be considered as a non-conservative force. This force may be created as follows:

$$\underline{G}_D = -\delta\,\underline{v}. \tag{8}$$

It follows that

$$\underline{G}_D = \delta[(\Omega Q_0 \sin \Omega t - L\dot{\theta} \cos\theta)\,\underline{i} + L\dot{\theta} \sin\theta\, \underline{j}]. \tag{9}$$

Along with this description, the system has one-degree-of freedom**,** and the generalized coordinate is represented by θ. Therefore, the generalized force is identified as:

$$Q = \underline{G}_D.\frac{\partial \underline{r}}{\partial \theta} = -\delta L^2\dot{\theta} + \delta\, \Omega L\, Q_0 \cos\theta \sin \Omega t. \tag{10}$$

From the elements of the analytical mechanics, Lagrange's equation with the non-conservative force may be written as:

$$\frac{d}{dt}\left(\frac{\partial \Re}{\partial \dot{\theta}}\right) - \frac{\partial \Re}{\partial \theta} = Q. \tag{11}$$

Inserting Eqs. (7) and (10) into Eq. (11), it follows that the governing equation of motion of the considered magnetic IP may be written as follows:

$$m\, L^2\ddot{\theta} + \delta\, L^2\dot{\theta} + k\theta - L\Omega Q_0(m\,\Omega \cos \Omega t + \delta\, \sin \Omega t)\, \cos\theta - L(mg + q\,B\,Q_0\Omega\, \sin \Omega t)\, \sin\theta = 0. \tag{12}$$

Equation (12) signifies the fundamental equation of motion with restoring as well as multi-parametric forces. This equation may be converted to a linear forcing Mathieu equation under the highest approximation of the restoring forces as follows:

$$mL^2\ddot{\theta} + \delta\, L^2\dot{\theta} - (mgL - k + q\,B\,L\,Q_0\Omega \sin \Omega t)\theta = Q_0 L\Omega(mL\Omega \cos \Omega t + \delta \sin \Omega t). \tag{13}$$

Analogous situations of Eq. (8) were previously presented in [27], and [28]. Now, let's return to the original controlling equation as given in Eq. (12). In what follows, a novel technique will be utilized to examine the stability standards of the magnetic IP. Before dealing with the mathematical analysis of the controlling equation of the IP as given in Eq. (12), a non-dimensional procedure will be needed for more convenience. For this objective, the non-dimensional procedure can be accomplished in numerous ways, based mainly on the selection of qualities. Let us consider the characteristic parameters: Q_0, $\sqrt{Q_0/g}$ and m stand for length, time, and mass, respectively. Along with these characteristics, Eq. (12) may be converted to the following non-dimensional form:

$$L^2\ddot{\theta} + \delta\, L^2\dot{\theta} + k\theta - L\Omega(\Omega \cos \Omega t + \delta\, \sin \Omega t)\, \cos\theta - L(1 + H\Omega \sin \Omega t)\, \sin\theta = 0, \tag{14}$$

where the parameter H refers to the non-dimensional term of the magnetic contribution, which results from the product $q\,B$.

3 An improved frequency evaluation

In what follows, the underlying aim is to achieve a uniform analytical estimate solution of the fundamental equation of motion as shown in Eq. (14). For the sake of simplicity of the mathematical procedure, approximations of the restoring forces sin θ and cos θ will be used, where sin $\theta \approx \theta - \frac{1}{6}\theta^3 + \ldots$ and cos $\theta \approx 1 - \frac{1}{2}\theta^2 + \ldots$. Therefore, Eq. (14) can be rewritten as

$$\begin{aligned}\ddot{\theta} + \delta\,\dot{\theta} + \omega^2\theta - \frac{\Omega\, H}{L}\, \sin \Omega t\ \theta + \frac{\Omega}{2L}(\Omega \cos \Omega t + \delta\, \sin \Omega t)\,\theta^2 \\ + \frac{1}{6L}(1 + \Omega\, H\, \sin \Omega t)\,\theta^3 - \frac{\Omega}{L}(\Omega \cos \Omega t + \delta\, \sin \Omega t) = 0,\end{aligned} \tag{15}$$

where $\omega^2 = (k - L)\big/ L^2$.

The following performance is based on a coupling of HPM and L_T as:

Equation (15) may be divided as:

$$I(\theta) = \ddot{\theta} + \omega^2\theta, \tag{16a}$$

and

$$N(\theta) = \delta\,\ddot{\theta} - \frac{\Omega\,H}{L}\,\sin\Omega t\;\theta + \frac{\Omega}{2L}(\Omega\cos\Omega t + \delta\,\sin\Omega t)\,\theta^2 + \frac{1}{6L}(1 + \Omega\,H\,\sin\Omega t)\,\theta^3 - \frac{\Omega}{L}\,(\Omega\cos\Omega t + \delta\,\sin\Omega t)\,. \tag{16b}$$

For this objective, it is convenient to assume the following initial conditions:

$$\theta(0) = 0, \quad \text{and}\;\; \dot{\theta}(0) = 1. \tag{17}$$

It follows that the Homotopy equation may be written as follows:

$$I(\theta) + \rho\,N(\theta) = 0;\;\; \rho \in [0,\;1], \tag{18}$$

where a synthetic incorporated factor is denoted by ρ. It is frequently referred to as the Homotopy parameter.

The HPM can offer a selection of approximate solutions, as was explicitly indicated in our earlier works [24] and [25]. One of these approaches results in a traditional solution with secular terms. Unfortunately, the removal of these secular terms produces a trivial solution that is not acceptable. Using the extended frequency hypothesis, an alternative approach generates solutions that are typically appropriate, however, the produced solutions do not fulfill the numerical ones. Therefore, the HPM must consequently be changed once more. The delayed parameter, which is more effective in avoiding bifurcations and reducing vibration, has a dominant influence on this situation. So, we can perform another examination. The basic Homotopy equation uses a novel expansion in place of the conventional one. As shown in our prior work [29], it is believed that $\theta(t,\,\rho)$ may be extended to another formula. Consequently, the following are the procedures to obtain the required solution:

The time-dependent function may be expressed as:

$$\theta(t;\,\rho) = e^{-\delta\rho t/2}(\theta_0(t) + \rho\,\theta_1(t) + ...). \tag{19}$$

As stated earlier, Eq. (18) reveals the homotopy expression for the equation under consideration. Since the normal frequency of the exiting prototype is ω^2. It should be noted that the value of the stiffness parameter needs to exceed the length of the IP in order to obtain real natural frequency. The subsequent stability standards will be established on the extended frequency evaluation [24]. In agreement with this methodology, an extended synthetic frequency σ^2 can be expressed as:

$$\sigma^2 = \omega^2 + \sum_{j=1}^{\infty} \rho^j \sigma_j, \tag{20}$$

where the factors σ_i will be calculated afterward, as a mixture of the previous qualities of the considered structure. This will be accomplished in order by ignoring secular terms [30–32].

Combining Eqs. (18)-(20), while taking over the Laplace transforms and taking into consideration the preliminary circumstances that are provided in Eq. (17), one gets

$$L_T\{\theta(t;\,\rho)\} = \frac{1}{s^2+\sigma^2} - \frac{\rho}{s^2+\sigma^2} L_T[\sigma_1\theta - \delta\,\ddot{\theta} - \frac{\delta}{2}t\,\ddot{\theta} - \frac{\delta}{2}t\sigma^2\,\theta + \rho\delta\,\dot{\theta} - \frac{\Omega\,H}{L}\,\theta\;\sin\Omega t + \frac{\Omega}{2L}(\Omega\cos\Omega t + \delta\,\sin\Omega t)\,\theta^2 + \frac{1}{6L}(1 + \Omega\,H\,\sin\Omega t)\,\theta^3 - \frac{\Omega}{L}(\Omega\cos\Omega t + \delta\,\sin\Omega t)]. \tag{21}$$

Employing the inverse transforms to Eq. (21), one realizes

$$\theta(t;\,\rho) = \frac{1}{\sigma}\sin\sigma\,t - L_T^{-1}\left\{\frac{\rho}{s^2+\sigma^2} L_T[\sigma_1\theta - \delta\,\ddot{\theta} - \frac{\delta}{2}t\,\ddot{\theta} - \frac{\delta}{2}t\sigma^2\,\theta + \rho\delta\,\dot{\theta} - \frac{\Omega\,H}{L}\,\theta\;\sin\Omega t + \frac{\Omega}{2L}(\Omega\cos\Omega t + \delta\,\sin\Omega t)\,\theta^2 + \frac{1}{6L}(1 + \Omega\,H\,\sin\Omega t)\,\theta^3 - \frac{\Omega}{L}(\Omega\cos\Omega t + \delta\,\sin\Omega t)]\right\}. \tag{22}$$

By using the development of the dependent function $\theta(t;\rho)$ as presented in Eq. (22), and later identifying the coefficients of comparable powers ρ on both sides, one gets

$$\rho^0 : \ \theta_0(t) = \frac{1}{\sigma}\sin\sigma t \ , \tag{23}$$

and

$$\begin{aligned}\rho : \theta_1(t) = -L_T^{-1}\{&\frac{1}{s^2+\sigma^2}L_T[\sigma_1\theta_0 - \delta\,\dot{\theta}_0 - \frac{\delta}{2}t\,\ddot{\theta}_0 - \frac{\delta}{2}t\sigma^2\,\theta_0 + \rho\delta\,\dot{\theta}_0 - \frac{\Omega\,H}{L}\,\theta_0\sin\Omega t \\ &+ \frac{\Omega}{2L}(\Omega\cos\Omega t + \delta\ \sin\Omega t)\theta_0^2 + +\frac{1}{6L}(1+\Omega\,H\ \sin\Omega t)\,\theta_0^3 - \frac{\Omega}{L}(\Omega\cos\Omega t + \delta\ \sin\Omega t)]\}.\end{aligned} \tag{24}$$

Usually, the consistent acceptable formula results from the removal of the secular terms. Consequently, the coefficient of the circular function $\sin\sigma t$ should be overlooked. This implementation produces the factor σ_1 as:

$$\sigma_1 = \frac{1}{8L\,\sigma^2}. \tag{25}$$

The regular solution at this point is provided by

$$\begin{aligned}\theta_1(t) = &-\frac{[2H(\sigma^2-\Omega^2)(9\sigma^2-\Omega^2)(16\sigma^2-\Omega^2-2)+\Omega^2(4\sigma^2-\Omega^2)(16\sigma^2-\Omega^2)(9\sigma^2-\Omega^2-3)]}{L\{3\sigma^4(91\Omega^4+192\sigma^4)+\Omega^2[\Omega^6-10\sigma^2(82\sigma^4+3\Omega^4)]\}}cos\sigma t \\ &-\frac{sin3\sigma t}{192\,L\sigma^5}+\frac{\{\sigma^4[64\delta(\Omega^4+\Omega^2)+9]+\Omega^2[\Omega^2-\sigma^2(10+576\delta\sigma^4)]\}}{64\,L\sigma^5(\Omega^2-9\sigma^2)(\Omega^2-\sigma^2)}sin\sigma t \\ &+\frac{1}{4\,L\sigma^2}\left[\frac{(4\sigma^2-1)\,\Omega}{(\sigma^2-\Omega^2)}(\Omega cos\Omega t-\delta sin\Omega t)+\frac{H(8\sigma^2-1)}{(4\sigma^2-\Omega^2)}cos(\sigma-\Omega)t\right] \\ &+\frac{\Omega}{8L\sigma^2}\left\{\frac{[\delta\,sin(2\sigma-\Omega)t-\Omega cos(2\sigma-\Omega)t]}{(3\sigma-\Omega)(\sigma-\Omega)}-\frac{[\delta\,sin(2\sigma+\Omega)t+\Omega cos(2\sigma+\Omega)t]}{(\sigma+\Omega)(3\sigma+\Omega)}\right\} \\ &+\frac{H\,\Omega}{48\,L\sigma^3}\left[\frac{cos(3\sigma+\Omega)t}{(2\sigma+\Omega)(4\sigma+\Omega)}-\frac{cos(3\sigma-\Omega)t}{(4\sigma-\Omega)(2\sigma-\Omega)}\right].\end{aligned} \tag{26}$$

As a consequence, the following is how the constrained approximation of the equation of motion provided in Eq. (14) can be formulated:

$$\theta(t) = \lim_{\rho\to 1} e^{-\delta\rho t/2}(\theta_0(t) + \rho\,\theta_1(t) + ...). \tag{27}$$

The arguments of the circular functions must actually have a valid value in order to yield the constrained estimated solution shown in Eq. (27). When Eq. (25) and Eq. (20) are combined for this goal, it implies that the synthesized frequency matches a certain distinctive equation. The computations revealed that this equation reflects a synthesized fourth-degree polynomial. One may write this equation as follows:

$$\sigma^4 - \omega^2\sigma^2 - \frac{1}{8L} = 0. \tag{28}$$

It is suitable to evaluate this solution with the numerical approach as established by RK4 to assess the practicality of the previous expanded frequency implications. The requirements for this implementation are listed below. Therefore, the RK4 is used to achieve the numerical solution of Eq. (14), and then the curves of Fig. 2 are drawn according to the following data:

$$k = 0.9,\ L = 0.5,\ H = 0.2,\ \Omega = 0.01,\ \delta = 0.1.$$

The computations demonstrated that the synthetic frequency has the amount $\sigma = 1.32038$ and the other roots (two are complex conjugate and the third is real and negative).

Equation (27) reads that the damped coefficient δ performs a dominant role in damping the solution. Therefore, it plays a major part in suppressing the instability of the IP. On the other hand, the curve of the time history of this solution has the form of decay behavior which means that this solution is stable and free of chaos, as seen in Fig. 2a. To confirm this conclusion, the corresponding phase plane plot is graphed in Fig. 2b,

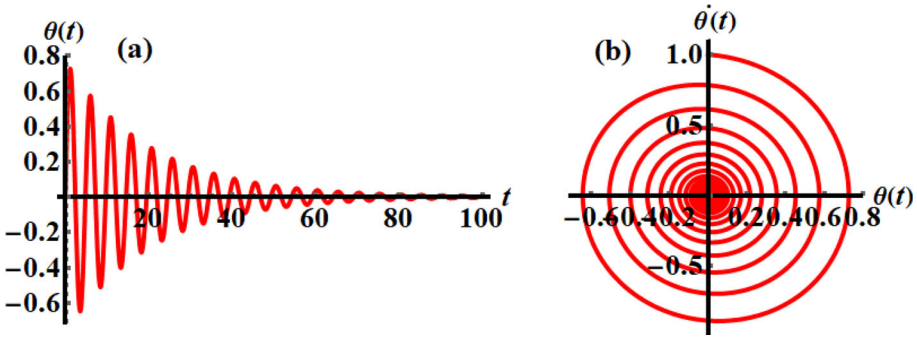

Fig. 2 Depicts **a** for the numerical solution, while **b** for corresponding to phase plane of Eq. (14)

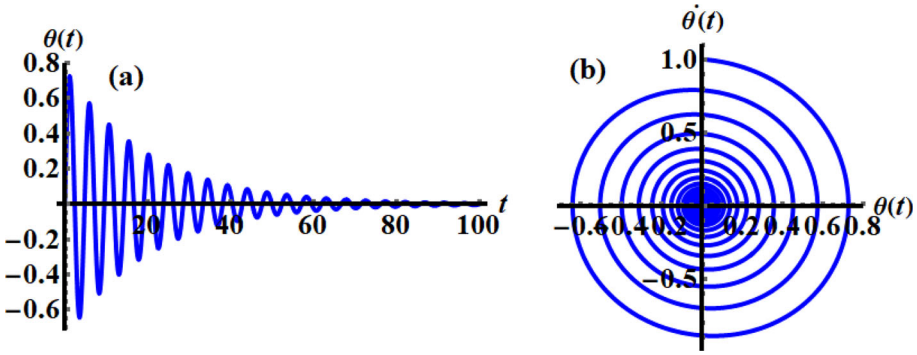

Fig. 3 **a** Shows the analytic solution, while **b** describes for the corresponding phase plane, of Eq. (27)

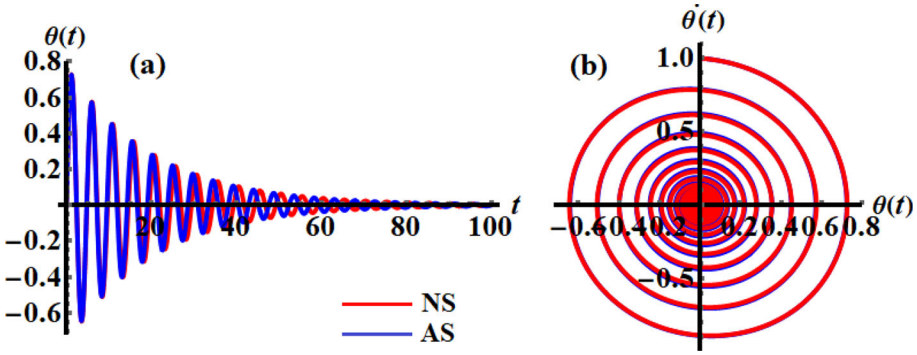

Fig. 4 Reveals the comparison between the NS and the AS: **a** for the time history, while **b** for the corresponding phase plane

which has the form of a spiral curve toward one point. On the contrary, considering the above data, the analytic solution (AS), as given by Eq. (27), is graphed in Fig. 3. The portions (a) and (b) of this picture display the temporal history of the AS and the phase plane of this solution, respectively. The comparison between the NS and the AS shows consistency as illustrated in portions (a) and (b) of Fig. 4. The inspection of this figure shows that the two curves are highly in accord. This means that the expanded frequency, as a systematic estimated solution, is a favorable and powerful perturbation procedure.

Examining the contours of Fig. 5 demonstrates the impact of the various values of the non-dimensional term of the magnetic field $H(= 0, 20, 40)$ on the time history of the obtained analytic solution and its phase plane plot when $k = 0.9$, $L = 0.5$, $\Omega = 0.01$, and $\delta = 0.1$. As previously interpreted, the waves have decay forms, but also the amplitude of the waves increases with the increase of H, as seen in Fig. 5a. Moreover, the decay rate of the drawn waves rises with the decrease of the amounts of H. The function H is drawn via its first derivative to yield the phase plane diagram, as seen in Fig. 5b. These curves have spiral forms, pointing toward one point, which indicates the stability of the obtained solution. Therefore, the magnetic field has a

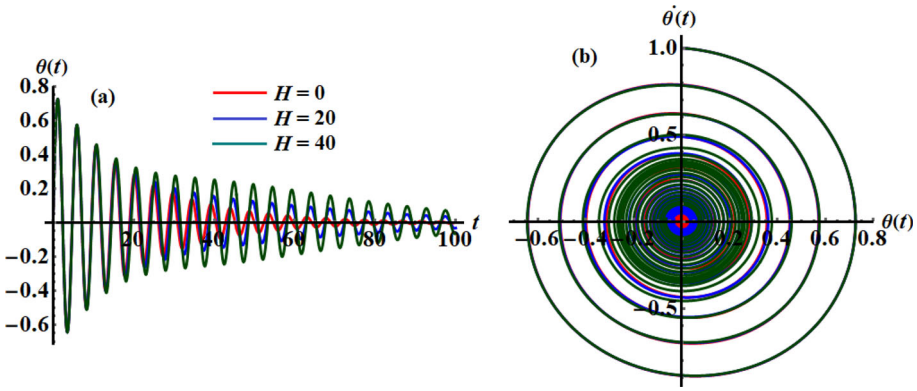

Fig. 5 Describes the variation of H, **a** for the analytic time history, and **b** for the corresponding the phase plane diagram of Eq. (27)

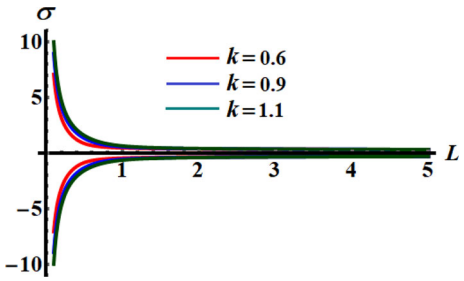

Fig. 6 Describes the influence of various values of k on the curves in the plane $\sigma - L$

substantial impact on the stability of the considered model, in which the decaying wave period increases for greater values of this field, in comparison to its lower values.

The curves of Fig. 6 represent the solution of Eq. (28) at various values of spring stiffness k. These curves have symmetric forms about the horizontal L axis. Therefore, these curves have a decayed form with the change of k, which implies the motion is stable.

4 Multiple time scale method

The multiple time scales method [27] is employed to accomplish the stability behavior of Eq. (15). One may contemplate that the dependent variable as a function t may be formulated in light of the HPM. Subsequently, rather than treating the expansion as a function of only one independent variable or scales, it is handled as a function of many time measures. In the perturbation theory, the methodology of multiple time scales is generally regarded as a further normative concept. To achieve this, one starts by including two additional independent variables in accordance with what follows:

$$T_n = \rho^n t, n = 0, 1, \ldots \tag{29}$$

In light of the derivatives, they will be transformed as:

$$\frac{\mathrm{d}}{\mathrm{d}t} \equiv \frac{\mathrm{d}T_0}{\mathrm{d}t}\frac{\partial}{\partial T_0} + \frac{\mathrm{d}T_1}{\mathrm{d}t}\frac{\partial}{\partial T_1} + \ldots = D_0 + \rho D_1 + \ldots, \tag{30}$$

$$\text{and } \frac{\mathrm{d}^2}{\mathrm{d}t^2} \equiv D_0^2 + 2\rho D_0 D_1 + \ldots, \tag{31}$$

where $D_n \equiv \frac{\partial}{\partial T_n}$.

The solution of Eq. (15) is assumed to be characterized as:

$$\theta(t;\rho) = \theta_0(T_0, T_1, \ldots) + \rho\theta_1(T_0, T_1, \ldots) + \ldots \tag{32}$$

It should be mentioned that the order of any function is determined by the number of independent time scales. In other words, if the construction is completed up to $O(\rho)$, then T_0 and T_1 are the essential requirements.

In light of the Homotopy perturbation, Eq. (15) may be written as follows:

$$\ddot{\theta}+\omega^2\theta+\rho\left[\delta\dot{\theta}-\frac{\Omega H}{L}\sin\Omega t\theta+\frac{\Omega}{2L}(\Omega\cos\Omega t+\delta\ \sin\Omega t)\,\theta^2+\frac{1}{6L}(1+\Omega\,H\ \sin\Omega t)\,\theta^3\right]$$
$$=\frac{\Omega}{L}(\Omega\cos\Omega t+\delta\sin\Omega t);\qquad\qquad \rho\in[0,\,1]. \tag{33}$$

For further suitability, to achieve a precise development, we carry out the extension up to $O(\rho)$. In this situation, only two-time scales, T_0 and T_1 are required.

Combining Eqs. (30)-(32) into Eq. (33), then connecting the amounts of similar powers of ρ, One gets the formulas shown as follows:

$$\rho^0:(D_0^2+\omega^2)\theta_0=\frac{\Omega}{L}(\Omega\cos\Omega T_0+\delta\sin\Omega T_0), \tag{34}$$

and

$$\rho:(D_0^2+\omega^2)\theta_1=-\left[2D_0D_1\theta_0+\delta D_0\theta_0-\frac{\Omega H}{L}\sin\Omega T_0\theta_0+\frac{\Omega}{2L}(\Omega\cos\Omega T_0+\delta\ \sin\Omega T_0)\theta_0^2+\frac{1}{6L}(1+\Omega\,H\ \sin\Omega T_0)\theta_0^3\right], \tag{35}$$

Through this methodology, it is straightforward to formulate the solution to Eq. (34) as follows:

$$\theta_0(T_0,\,T_1)=A(T_1)e^{i\omega T_0}+\overline{A}(T_1)e^{-i\omega T_0}-\frac{\Omega}{2L(\Omega^2-\omega^2)}[e^{iT_0\Omega}(\Omega-i\delta)+e^{-iT_0\Omega}(\Omega+i\delta)], \tag{36}$$

where A is an unspecified complex function that can be established later and $\overline{A}$ is a corresponding complex conjugate.

Substituting Eq. (36) into Eq. (35), one finds

$$(D_0^2+\omega^2)\theta_1=\left\{\frac{\Omega^2(\delta^2+\Omega^2)[2L(\Omega^2-\omega^2)-1]-4iL^3\delta\omega(\omega^2-\Omega^2)^2}{4L^3(\omega^2-\Omega^2)^2}A(T_1)-\frac{A^2(T_1)\overline{A}(T_1)}{2L}-\frac{1}{2}i\omega D_1A(T_1)\right\}e^{i\omega T_0}$$
$$+N.S.T.+c.c. \tag{37}$$

wherever $c.c.$ signifies the complex conjugate of the previous relationships**,** and NST describes the terms that do not generate secular terms.

The necessary consistent development of the function $\theta_1(T_0,\,T_1)$ can be achieved by eliminating the secular term. The resources of this secular term come from the coefficients of the exponential $e^{\pm i\omega T_0}$. Consequently, the uniform valid expansion necessitates that

$$\frac{\Omega^2(\delta^2+\Omega^2)[2L(\Omega^2-\omega^2)-1]-4iL^3\delta\omega(\omega^2-\Omega^2)^2}{4L^3(\omega^2-\Omega^2)^2}A(T_1)-\frac{A^2(T_1)\overline{A}(T_1)}{2L}-2i\omega D_1A(T_1)=0. \tag{38}$$

Equation (38) is frequently referred to as the amplitude equation and is well recognized as the solvability criterion.

4.1 Examination of stability in the non-resonance situation

Let's return to the solvability requirement provided in Eq. (38) for the non-resonance case to examine the stability outline. In reality, the unidentified function $A(T_1)$ might be defined in terms of the time-independent factor T_1 using this equation. Furthermore, the structure of this function is heavily influenced by this factor. For this purpose, Eq. (37) is partially integrated in relation to the parameter. One may return to the initial time-independent variable in a subsequent process. Remember that the complex function is not a function of time. Of course, doing so requires multiplying Eq. (38) by ρ. Therefore, the amplitude equation can be transformed into $dA\big/dt$. To this end, one could arrive at the amplitude equation shown as follows:

$$2i\omega\frac{dA(t)}{dt}-[\frac{\Omega^2(\delta^2+\Omega^2)[2L(\Omega^2-\omega^2)-1]-4iL^3\delta\omega(\omega^2-\Omega^2)^2}{4L^3(\omega^2-\Omega^2)^2}]A(T_1)-\frac{A^2(T_1)\overline{A}(T_1)}{2L}=0. \tag{39}$$

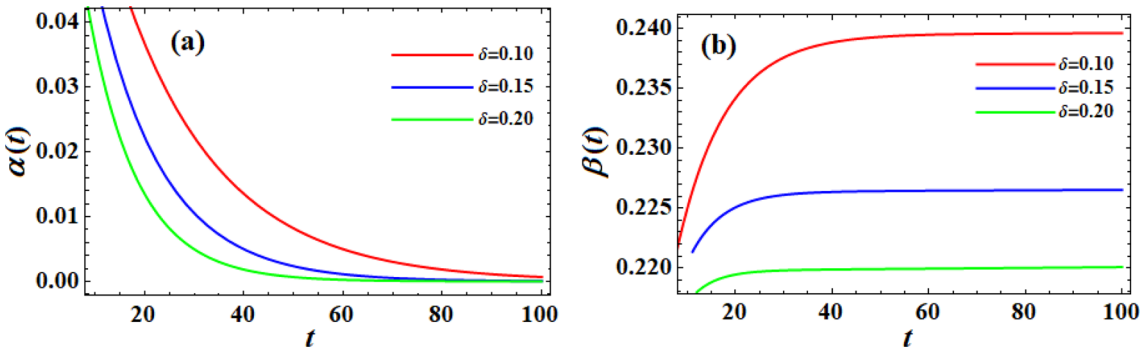

Fig. 7 Describes the temporal histories when $\delta(= 0.1, 0.15, 0.2)$: **a** for the function α and **b** for the function β

Having complex coefficients, Eq. (39) is a first-order nonlinear differential equation. In the non-resonant case, this amplitude equation would regulate the stability fundamental to the current issue. The accompanying polar form procedure can be used to determine the solution to this equation:

$$A(t) = \alpha(t)e^{i\beta}(t), \tag{40}$$

where $\alpha(t)$ and $\beta(T)$ are two real functions.

The two additional algebraic equations result from the process of reorganizing Eq. (59) into Eq. (58) and evaluating the real and imaginary components through both sides:

$$8\omega\beta'(t) - \frac{2\alpha(t)^2}{L} + \frac{\Omega^2(\delta^2+\Omega^2)(2L\Omega^2 - 1 - 2L\omega^2)}{L^3(\omega^2-\Omega^2)^2}\alpha(t) = 0, \tag{41}$$

$$\text{and} \quad \delta\alpha(t) + 2\alpha'(t) = 0. \tag{42}$$

The solutions of Eqs. (41) and (42) reveal the following functions:

$$\alpha(t) = c_1 \mathrm{e}^{-\frac{\delta t}{2}}, \quad \text{and} \quad \beta(t) = c_2 - \frac{c_1^2 \mathrm{e}^{-\delta t}}{4L\delta\omega} + \frac{\Omega^2(\delta^2+\Omega^2)(1+2L\omega^2-2L\Omega^2)t}{8L^3\omega(\omega^2-\Omega^2)^2}. \tag{43}$$

As a result, stability exists even in the non-resonant situation assuming that

$$\delta \geq 0. \tag{44}$$

An examination of the curves in Fig. 7 demonstrates the time histories of the functions α and β. This figure is drawn when $k = 0.9$, $L = 0.5$, $H = 0.2$, and $\Omega = 0.01$ for the values of the damping parameter $\delta(= 0.1, 0.15, 0.2)$. It is shown that the curves of α function have a decaying behavior with the variation of δ values as seen from Fig. 7a. On the contrary, the variation of the function β with time when δ varies is graphed in Fig. 7b, where the curves of this function increase to certain values and then become stationary till the end of time interval. The plotted curves of Fig. 7 are aligned with the mathematical formula (43) of the functions α and β.

4.2 Evaluation of stability in the resonance situation

As realized in the preceding Section, the stability standards of the non-resonance situation do not consider all such characteristics. The investigation that follows tackles the resonance cases. Interestingly, the choice to use non-homogeneous periodic terms all across the zero-order equation results in a large number of resonance occurrences. Such resonance situations can be divided into super-harmonic and sub-harmonic ones, with the following list:

- *Sub-Harmonic Resonance*
  (1) As $\Omega \approx \omega$, the coefficients of the exponentials $e^{i\Omega T_0}$, $e^{i(2\Omega-\omega)T_0}$ and $e^{i(2\omega-\Omega)T_0}$ become secular terms.
  (2) As $\Omega \approx 2\omega$, the coefficient of the exponential $e^{i(3\omega-\Omega)T_0}$ becomes secular terms.
  (3) As $\Omega \approx 3\omega$, the coefficient of the exponential $e^{i(\Omega-2\omega)T_0}$ becomes a secular term.

(4) As $\Omega \approx 4\omega$, the coefficient of the exponential $e^{i(3\omega-\Omega)T_0}$ becomes a secular term.

- *Super-Harmonic Resonance*

(1) As $\Omega \approx \omega/2$, the coefficients of the exponentials $e^{2i\Omega T_0}$ and $e^{i(2\omega-2\Omega)T_0}$ become secular term s .
(2) As $\Omega \approx \omega/3$, the coefficient of the exponential $e^{3i\Omega T_0}$ becomes a secular term.
(3) As $\Omega \approx \omega/4$, the coefficient of the exponential $e^{4i\Omega T_0}$ becomes a secular term.
(4) As $\Omega \approx 3\omega/2$, the coefficient of the exponential $e^{i(2\Omega-2\omega)T_0}$ becomes a secular term.
(5) As $\Omega \approx 2\omega/3$, the coefficient of the exponential $e^{i(3\Omega-\omega)T_0}$ becomes a secular term.

The resonance case has a benefit when used. It aids in the introduction of non-secular terms. The present review only addresses one of these resonance situations in order to shorten the computations for the sub- and super-harmonic resonances. For instance, we are going to examine only two cases**:** one for the sub-harmonic resonance which is $\Omega \approx 3\omega$ and the other for the super-harmonic resonance which is $\Omega \approx 3\omega/2$.

To investigate one case of the sub-harmonic resonance, the quantitative nearness of Ω to 3ω is studied while proposing a detuning factor ε to get

$$\Omega = 3(\omega + \rho\varepsilon), \tag{45}$$

Here, one gets

$$i(\Omega - 2\omega)T_0 = i\omega T_0 + 3i\varepsilon T_1. \tag{46}$$

Consequently, the secular terms will commence increasing. At this point, the solvability requirement provided by Eq. (38) will be changed to read as:

$$2i\omega D_1 A(T_1) - \left[\frac{\Omega^2(\delta^2+\Omega^2)[2L(\Omega^2-\omega^2)-1]-4iL^3\delta\omega(\omega^2-\Omega^2)^2}{4L^3(\omega^2-\Omega^2)^2}\right]A(T_1) + \frac{A^2(T_1)\overline{A}(T_1)}{2L} - \frac{\Omega(\Omega-i\delta)(1+L\omega^2-L\Omega^2)\overline{A}^2(T_1)}{4L^2(\omega^2-\Omega^2)}e^{3i\varepsilon T_1} = 0. \tag{47}$$

Similar to the reasons presented in the non-resonance example, one observes

$$2i\omega\frac{dA(t)}{dt} - \left[\frac{\Omega^2(\delta^2+\Omega^2)[2L(\Omega^2-\omega^2)-1]-4iL^3\delta\omega(\omega^2-\Omega^2)^2}{4L^3(\omega^2-\Omega^2)^2}\right]A(t) + \frac{A^2(t)\overline{A}(t)}{2L} - \frac{\Omega(\Omega-i\delta)(1+L\omega^2-L\Omega^2)\overline{A}^2(t)}{4L^2(\omega^2-\Omega^2)}e^{3i\varepsilon t} = 0. \tag{48}$$

Equation (48) is a complex and variable first-order nonlinear differential equation. The following is how to find its solution:

$$A(t) = \lambda e^{i\varepsilon t}, \tag{49}$$

where λ and ε are real constants.

Equating the real and imaginary terms after substituting Eq. (49) into Eq. (48), one gets

$$L(\Omega^2-\omega^2)\{\Omega^2(2\delta^2+\lambda+2\Omega^2)+L(\Omega^2-\omega^2)[8L\varepsilon\omega-\lambda(2\lambda+\Omega^2)]\}-\Omega^2(\delta^2+\Omega^2)=0, \tag{50}$$

$$\text{and}\quad \left(L\lambda\Omega-4L^2\omega\right)\left(\omega^2-\Omega^2\right)+\lambda\Omega=0. \tag{51}$$

The solutions of Eqs. (50) and (51) generate

$$\begin{aligned}\lambda &= \frac{4L^2\omega(\omega^2-\Omega^2)}{\Omega(1+L\omega^2-L\Omega^2)},\\ \varepsilon &= \{4L^4\omega(\omega^2-\Omega^2)^3[2\Omega^3+4L(\omega^2-\Omega^2)(8\mathrm{L}\,\omega+\Omega^3)]+\Omega^4(\delta^2+\Omega^2)\\ &\quad\times[1+L(\omega^2-\Omega^2)(4+5L^2(\omega^2-\Omega^2))]+2L^3\Omega^3(\omega^2-\Omega^2)^2[2\omega\\ &\quad+\Omega(\delta^2+\Omega^2)(\omega^2-\Omega^2)]\}/\{8L^3\omega(\omega^2-\Omega^2)^2\Omega^2[1+L(\omega^2-\Omega^2)]^2\}.\end{aligned} \tag{52}$$

Equations in the system (52) are graphed in the planes $\Omega\lambda$ and $\Omega\varepsilon$ to yield parts (a) and (b) of Fig. 8, respectively. The influence of different amounts of L on the behavior of the plotted curves is consistence with these equations.

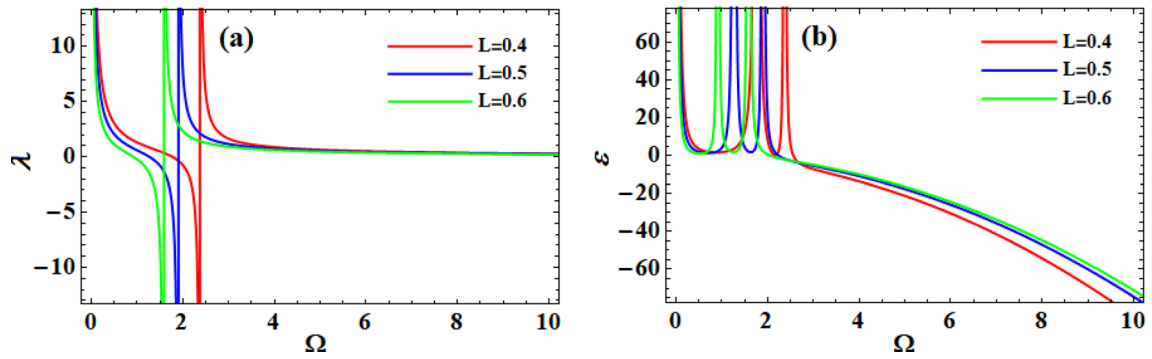

Fig. 8 Shows the influence of the various values of $L(= 0.4, 0.5, 0.6)$: **a** in the plane $\Omega\lambda$ and **b** in the plane $\Omega\varepsilon$

- *Super-harmonic resonance*

The quantitative nearness of Ω to $3\omega/2$ yields

$$\Omega = \frac{3}{2}(\omega + \rho\mu). \tag{53}$$

where μ is a new detuning parameter. In this case, one finds

$$2i(\Omega - \omega)T_0 = i\omega T_0 + 3i\mu T_1. \tag{54}$$

Consequently, secular terms will start increasing. At this point, the solvability requirement provided by Eq. (38) will be changed to read as:

$$2\mathrm{i}\omega D_1 A(T_1) - \frac{\Omega^2(\delta^2+\Omega^2)[2L(\Omega^2-\omega^2)-1] - 4iL^3\delta\omega(\omega^2-\Omega^2)^2}{4L^3(\omega^2-\Omega^2)^2}A(T_1) + \frac{A^2(t)\overline{A}(T_1)}{2L} + \frac{H(\delta+i\Omega)\Omega^2\overline{A}^2(T_1)}{8L^2(\omega^2-\Omega^2)}\mathrm{e}^{3i\mu T_1} = 0. \tag{55}$$

Corresponding to the justifications presented in the non-resonance situation, one observes

$$2i\omega\frac{\mathrm{d}A(t)}{dt} - \frac{\Omega^2(\delta^2+\Omega^2)[2L(\Omega^2-\omega^2)-1] - 4iL^3\delta\omega(\omega^2-\Omega^2)^2}{4L^3(\omega^2-\Omega^2)^2}A(t) + \frac{A^2(t)\overline{A}(t)}{2L} + \frac{H(\delta+i\Omega)\Omega^2\overline{A}^2(t)}{8L^2(\omega^2-\Omega^2)}\mathrm{e}^{3i\mu t} = 0. \tag{56}$$

Equation (56) is a first-order nonlinear differential equation with complex and variable coefficients. Its solution may be obtained as follows:

$$A(t) = \eta e^{i\mu t}, \tag{57}$$

where η and μ are any two real amounts.

Replacing Eq. (57) into Eq. (56), and then comparing the real and imaginary relationships, one realizes

$$(\omega^2-\Omega^2)^2(4L^2\eta^2 - 16L^3\mu\omega) + 2\Omega^2(\delta^2+\Omega^2) + L\Omega^2(\omega^2-\Omega^2)(4\delta^2 - H\delta\eta + 4\Omega^2) = 0, \tag{58}$$

$$\text{and } L(\omega^2-\Omega^2)[8L^2\delta\omega(\omega^2-\Omega^2) - H\eta\Omega^3] = 0, \tag{59}$$

The solutions of Eqs. (58) and (59) produce

$$\eta = \frac{8L^2\delta\omega(\omega^2-\Omega^2)}{H\Omega^3} \tag{60}$$

$$\text{and } \mu = \frac{\Omega^2(\delta^2+\Omega^2)}{8L^2\omega(\omega^2-\Omega^2)}\left[2 + \frac{1}{L(\omega^2-\Omega^2)}\right] + \frac{16L^3\delta^2\omega(\omega^2-\Omega^2)^2}{H^2\Omega^6} - \frac{\delta^2}{2\Omega}. \tag{61}$$

The above two Eqs. (60) and (61) are graphed in the parts (a) and (b) of Fig. 9 when considering the same values of $k = 0.9$ and $H = 0.2$ when $L(= 0.14, 0.5, 0.6)$. It is obvious that the included curves in Fig. 9a decrease till a certain value of Ω and then they have a stationary manner over time. On the other hand, curves of Fig. 9b start from higher values of μ and then oscillates between decreasing and increasing till $\Omega = 2$. Finally, they behave decreasing manner till the end of time period.

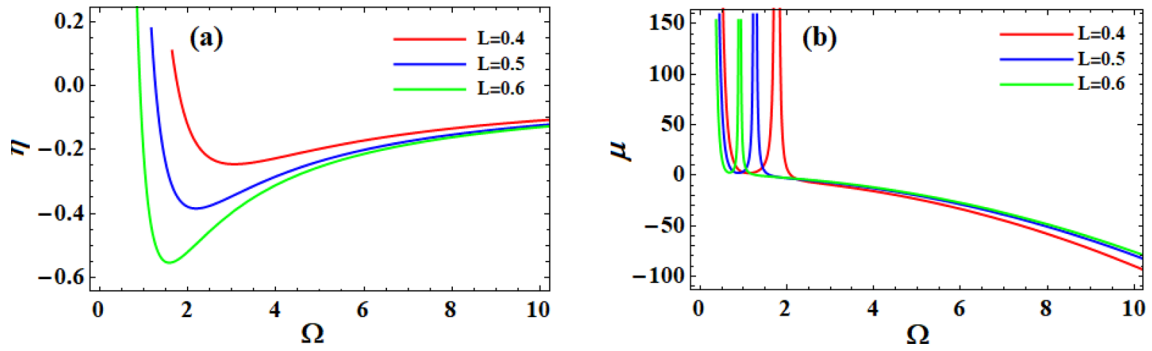

Fig. 9 Shows the impact of the various values of $L(= 0.4, 0.5, 0.6)$: **a** in the plane $\Omega\eta$ and **b** in the plane $\Omega\mu$

5 Concluding remarks

The current work examines the base periodic motion of an IP to achieve the stability structure IP. A steady magnetic field has an impact on the motion normal to the plane configuration. Additionally, a non-conservative force that dampens air is considered. The traditional analytical mechanics is employed to derive its fundamental equation of motion. In order to get rid of the restoring forces, the Taylor theory is utilized for simplifying the mathematical analysis. To provide a nearly appropriate periodic solution, the modified HPM is applied. A numerical approach based on RK4 is employed to support the earlier finding. The graphs of the two solutions are very similar to one another, proving better accuracy of the perturbation technique. There is a strong agreement between the analytical and numerical schemes when they are compared. The solution time history curve displays a decaying behavior, demonstrating stability and the absence of chaos. Utilizing the time scale approach, resonance and non-resonance cases are discovered during the stability investigation. The concept of multiple time scales is actually recognized as a further conventional approach in all perturbation approaches. The cases of sub- and super-harmonic resonances are examined. Certain graphical representations are used to demonstrate the influence of the characteristic physical factors and to demonstrate the behavior of the obtained solution. To show how the behavior of the obtained solution is influenced by the typical physical parameters, some graphical representations are employed. It has been found that increasing the spring torsional consistent stiffness and the damped coefficient can improve the statically unstable IP instability. Additionally, the magnetic field has an important impact on the stability of the investigated model, which explains why the time of the decaying waves increases with higher values of this field, relative to smaller values of the field. It can therefore be used in a variety of engineering devices that require a certain time to become more stable.

Author contributions GMM contributed to conceptualization, resources, formal analysis, writing—original draft preparation, visualization and reviewing. TSA contributed to investigation, methodology, data curation, visualization, reviewing and editing. MHZ contributed to investigation, visualization, methodology, conceptualization, and validation.

Funding Open access funding provided by The Science, Technology & Innovation Funding Authority (STDF) in cooperation with The Egyptian Knowledge Bank (EKB). There was no specific grant for this research from any funding source in the public, private, or non-profit sectors.

Data availability The datasets used and/or analyzed during the current study available from the corresponding author on reasonable request.

Declarations

Conflict of interest There are no competing interests declared by the authors.

References

1. Xu, C., Yu, X.: Mathematical modeling of elastic inverted pendulum control system. J. Control Theory Appl. **3**, 281–282 (2004)
2. Huang, X., Wen, F., Wei, Z.: Optimization of triple inverted pendulum control process based on motion vision. EURASIP J. Image Video Process. **2018**, 73 (2018)
3. Aranovskiy, S.V., Biryuk, A.E., Nikulchev, E.V., Ryadchikov, I.V., Sokolov, D.V.: Observer design for an inverted pendulum with biased position sensors. J. Comput. Syst. Sci. Int. **58**(2), 297–304 (2019)
4. He, J., Cui, L., Sun, J., Huang, P., Huang, Y.: Chaotic dynamics analysis of double inverted pendulum with large swing angle based on Hamiltonian function. Nonlinear Dyn. **108**(4), 4373–4384 (2022)
5. Guo, C., Luo, C.J.A.: Periodic motions on bifurcation trees in an inverted pendulum with a periodically moving base. Int. J. Dyn. Control (2020). https://doi.org/10.1007/s40435-020-00647-6
6. Dolatabad, M.R., Pasharavesh, A., Khayyat, A.A.A.: Analytical and experimental analyses of nonlinear vibrations in a rotary inverted pendulum. Nonlinear Dyn. **107**, 1887–1902 (2022)
7. Zhang, X.-L., Fan, H.-M., Zang, J.-Y., Zhao, L., Hao, S.: The stabilization and 3D visual simulation of the triple inverted pendulum based on CGA-PIDNN. Int. J. Control Autom. Syst. **13**(4), 1010–1019 (2015)
8. Johnson, T., Zhou, S., Cheah, W., Mansell, W., Young, R., Watson, S.: Implementation of a perceptual controller for an inverted pendulum robot. J. Intell. Rob. Syst. **99**, 683–692 (2020)
9. Nayfeh, A.H., Mook, D.T.: Nonlinear Oscillations. Wiley, New York (1979)
10. Meirovitch, L.: Methods of Analytical Dynamics. Dover Publication, New York (2003)
11. Habib, G., Giorgi, G., Davidson, J.: Coexisting attractors in floating body dynamics undergoing parametric resonance. Acta Mec. **233**(6), 2351–2367 (2022)
12. Amer, T.S., Bek, M.A., Nael, M.S., Sirwah, M.A., Arab, A.: Stability of the dynamical motion of a damped 3DOF auto-parametric pendulum system. J. Vib. Eng. Technol. **10**(5), 1883–1903 (2022)
13. Amer, T.S., Starosta, R., Almahalawy, A., Elameer, A.S.: The stability analysis of a vibrating auto-parametric dynamical system near resonance. Appl. Sci. **12**, 1737 (2022). https://doi.org/10.3390/app12031737
14. He, J.-H., Amer, T.S., Abolila, A.F., Galal, A.A.: Stability of three degrees-of-freedom auto-parametric system. Alex. Eng. J. **61**(11), 8393–8415 (2022). https://doi.org/10.1016/j.aej.2022.01.064
15. Amer, T.S., Abady, I.M., Farag, A.M.: On the solutions and stability for an auto-parametric dynamical system. Arch. Appl. Mech. **92**, 3249–3266 (2022)
16. Yakubu, G., Olejnik, P., Awrejcewicz, J.: On the modeling and simulation of variable-length pendulum systems: a review. Arch. Comput. Methods Eng. **29**, 2397–2415 (2022)
17. Liu, Y., Qin, Z., Chu, F.: Nonlinear forced vibrations of rotating cylindrical shells under multi-harmonic excitations in thermal environment. Nonlinear Dyn. **108**(4), 2977–2991 (2022)
18. Zhang, W., Ma, L., Zhang, Y.F., Behdinan, K.: Nonlinear and dual-parameter chaotic vibrations of lumped parameter model in blisk under combined aerodynamic force and varying rotating speed. Nonlinear Dyn. **108**, 1217–1246 (2022)
19. Zhang, Y., Song, W., Yin, H., Ma, J.: Improved homotopy perturbation solution for nonlinear transverse vibration of orthotropic membrane. J. Vib. Eng. Technol. **10**, 995–1005 (2022)
20. He, J.H.: Homotopy perturbation technique. Comput. Methods Appl. Mech. Eng. **178**, 257–262 (1999)
21. Ganji, D.D.: The application of He's homotopy perturbation method to nonlinear equation arising in heat transfer. Phys. Lett. A **355**, 337–341 (2006)
22. Moatimid, G.M., Amer, T.S.: Analytical solution for the motion of a pendulum with rolling wheel: stability analysis. Sci. Rep. **12**, 12628 (2022)
23. Moatimid, G.M., Amer, T.S.: Analytical approximate solutions of a magnetic spherical pendulum: stability analysis. J. Vib. Eng. Technol. (2022). https://doi.org/10.1007/s42417-022-00693-8
24. Moatimid, G.M.: Stability analysis of a parametric Duffing oscillator, Stability analysis of a parametric Duffing oscillator. J. Eng. Mech. **146**(5), 0502001 (2020)
25. Moatimid, G.M.: Sliding bead on a smooth vertical rotated parabola: stability configuration. Kuwait J. Sci. **47**(2), 6–21 (2020)
26. Eyal, O., Goldstein, A.: Gauss' law for moving charges from first principles. Results Phys. **14**, 102454 (2019)
27. Nayfeh, A.H.: Introduction to Perturbation Techniques. John Wiley & Sons Inc., New Jersey (1981)
28. El-Dib, Y.O., Moatimid, G.M.: Stability configuration of a rocking rigid rod over a circular surface using the homotopy perturbation method and Laplace transform. Arab. J. Sci. Eng. **44**, 6581–6591 (2019)
29. Moatimid, G.M., Amer, T.S.: Nonlinear suppression using time-delayed controller to excited Van der Pol-Duffing oscillator: analytical solution techniques. Arch. Appl. Mech. (2022). https://doi.org/10.1007/s00419-022-02246-7
30. El-Sabaa, F.M., Amer, T.S., Gad, H.M., Bek, M.A.: On the motion of a damped rigid body near resonances under the influence of harmonically external force and moments. Results Phys. **19**, 103352 (2020)
31. Amer, W.S., Amer, T.S., Starosta, R., Bek, M.A.: Resonance in the cart-pendulum system-an asymptotic approach. Appl. Sci. **11**(23), 11567 (2021)
32. Amer, T.S., Abdelhfeez, S.A., Elbaz, R.F.: Modeling and analyzing the motion of a 2DOF dynamical tuned absorber system close to resonance. Arch. Appl. Mech. **93**, 785–812 (2023)